Bayesian Inference-Based Estimation of Normal Aortic, Aneurysmal and Atherosclerotic Tissue Mechanical Properties: From Material Testing, Modeling and Histology

Shuo Wang, Aziz Tokgoz, Yuan Huang, Yongxue Zhang, Jiaxuan Feng, Priya Sastry ⓘ, Chang Sun ⓘ, Nichola Figg, Qingsheng Lu, Michael P. F. Sutcliffe, Zhongzhao Teng ⓘ, and Jonathan H. Gillard

Abstract—Objective: **Mechanical properties of healthy, aneurysmal, and atherosclerotic arterial tissues are essential for assessing the risk of lesion development and rupture. Strain energy density function (SEDF) has been widely used to describe these properties, where material constants of the SEDF are traditionally determined using the ordinary least square (OLS) method. However, the material constants derived using OLS are usually dependent on initial guesses.** *Methods:* **To avoid such dependencies, Bayesian inference-based estimation was used to fit experimental stress-stretch curves of 312 tissue strips from 8 normal aortas, 19 aortic aneurysms, and 21 carotid atherosclerotic plaques to determine the constants, C_1, D_1, and D_2 of the modified Mooney-Rivlin SEDF.** *Results:* **Compared with OLS, material constants varied much less with *prior* in the Bayesian inference-based estimation. Moreover, fitted material constants differed amongst distinct tissue types. Atherosclerotic tissues associated with the biggest D_2, an indicator of the rate of increase in stress during stretching, followed by aneurysmal tissues and those from normal aortas. Histological analyses showed that C_1 and D_2 were associated with elastin content and details of the collagen configuration, specifically, waviness and dispersion, in the structure.** *Conclusion:* **Bayesian inference-based estimation robustly determines material constants in the modified Mooney-Rivlin SEDF and these constants can reflect the inherent physiological and pathological features of the tissue structure.** *Significance*: **This study suggested a robust procedure to determine the material constants in SEDF and demonstrated that the obtained constants can be used to characterize tissues from different types of lesions, while associating with their inherent microstructures.**

*Index Terms—*Aneurysm, artery, atherosclerosis, Bayesian, material constant, regression.

ABBREVIATIONS

CVD	Cardiovascular diseases.
Eq	Equation.
EVG	Elastin Van Gieson.
FC	Fibrous cap.
IPH/T	Intraplaque haemorrhage/thrombus.
MCMC	Markov Chain Monte Carlo.
MMP	Matrix metalloproteinase.
OLS	Ordinary least square.
SEDF	Strain energy density function.

NOMENCLATURE

W	Strain energy density function.
C_1, D_1, D_2	Modified Mooney-Rivlin model material constants.
I_1	First invariant of the left Cauchy-Green deformation tensor.
ξ	Lagrangian multiplier.
J	Determinant of the deformation gradient.
σ_{11}	Cauchy stress along the tensile direction.
λ	Stretch ratio.
$S(C_1, D_1, D_2)$	Objective function of the ordinary least squares method.
γ	Relative error.
$\boldsymbol{\theta}$	Unknown parameters in Bayesian inference-based estimation.
$\mathcal{D}$	Experimental data in Bayesian inference-based estimation.

$p(\boldsymbol{\theta}\|\mathcal{D})$	Conditional distribution of unknown parameters.
$p(\boldsymbol{\theta})$	Prior distribution.
$p(\mathcal{D}\|\boldsymbol{\theta})$	Likelihood function.
$p(\mathcal{D})$	Probability of the evidence.
$\mathcal{N}(0, \varepsilon^2)$	Gaussian noise.
ε	Standard deviation of Gaussian distribution.
κ	Dispersion of fibre orientations.
ω	Waviness of fibres.

I. INTRODUCTION

CARDIOVASCULAR diseases (CVD) are the No.1 killer and responsible for an estimated 31% of all deaths worldwide [1]. About 80% of all CVD deaths are due to heart attacks and strokes [1], which are induced by atherosclerotic plaques. Aortic aneurysms, occurring in approximately 8% of men aged >65 [2], are another common cause of CVD deaths, with the mortality after aneurysm rupture being ~90% [3]. In the current clinical practice, luminal stenosis and maximum wall diameter are the only validated risk assessment criteria for atherosclerotic disease and aneurysm, respectively. However, such size-based criteria showed only limited sensitivity and specificity [4]–[7]. Therefore, there is a clear need for novel risk-stratification biomarkers to estimate the risks of atherosclerosis and aneurysm in the hope of improving patient outcomes.

Under physiological conditions, both lesions are subject to mechanical loading due to dynamic blood pressure and flow. It has been shown that mechanical loading within the arterial tissue structure has an association with biological activities within the lesion [8]–[12], which can promote its development [13]–[15], leading to both progression and rupture. Accurate characterisation of mechanical properties of atherosclerotic and aneurysmal tissues is required for reliable prediction of mechanical loading in the lesion structure. A reliable prediction process should follow the steps of: (1) direct measurement of tissue stress-stretch [16]; (2) carefully selected strain energy density function (SEDF) [17]; and (3) determination of material constants in SEDF with an optimization method to minimise the objective function, which describes the difference between the predicted and measured stress-stretch curves. Several SEDFs have been used to characterize the tissue material [17]. It is challenging to obtain a robust estimation of material constants in an SEDF with traditional least squares methods, which often converge to a local minimum of the objective function in a narrow region around the initial guesses. This yields different sets of constants that can all fit the experimental data well. Although these distinct sets of material constants can lead to very similar stress predictions [17], it is inappropriate to characterise the tissue mechanical behaviour by using regressed material constants, whose values are highly dependent on their initial guesses. In other words, it is incorrect to assign a physical meaning to these regressed constants.

In this study, Bayesian inference was used to estimate the probability of each material constant across a wide range and the expectation was used to characterise the material constants for each tissue strip. This approach avoids non-uniqueness of parameter estimation associated with the least squares method. The uniqueness of the fitted material constants allows identification of the physical meaning of each constant and enable comparisons between the obtained parameters among distinct samples. The correlation of those parameters with the corresponding microscopic structures can also be investigated. The capability of the determined material constants to differentiate tissues from normal aorta, carotid atherosclerotic plaque and aortic aneurysm were assessed and the association between determined material constants and fibre architectures in the tissue was explored in this study.

II. MATERIALS AND METHODS

A. Collection of Tissue Samples and Material Testing

In this study, stress-stretch curves from direct material testing with 8 normal aortas [18], 19 aortic aneurysms [18] and 21 carotid atherosclerotic plaques [16] were collected from previous studies, except for 8 aneurysms. The eight aneurysmal samples (Seven males and one female, ages 63.3 ± 11.7 years) were collected from the Royal Papworth Cambridge University Hospital (Papworth Hospital) and three of them are from dissection at the arch. The protocol was approved by the local ethics committee and written informed consent was obtained from all patients.

Details of patient demographics except for the eight from Papworth Hospital, tissue preparation and testing protocol have been described in two previous studies [16], [18]. In brief, tissue strips from different components with dimensions ~1 × 1.5 × 10 mm³ (thickness×width×length) were prepared. Waterproof markers were placed on the tissue surface and each strip was mounted on an in-house designed micro tester with sandpaper attached to both ends. After pre-conditioning, the strip was pulled slowly until failure with the force and position of markers recorded. A displacement rate of 0.01 mm·s⁻¹ was used in all tensile tests. The stress-stretch curve of each strip was then derived from the recorded signals, considering the initial dimensions and by assuming incompressibility. The initial width and thickness of the sample strips were measured from high-resolution images with ruler calibration. Edge detections were performed in MATLAB (MathWorks, Inc.) to identify the edges. The thickness/width of each strip was determined by the average value of the distances between 100 pairs of closest points with an equal distance along each edge.

B. Strain Energy Density Function

In this study, the modified Mooney-Rivlin SEDF was used to characterise the mechanical behaviour of the tissue strips based on the consideration of material stability [17],

$$W = C_1\left(\bar{I}_1 - 3\right) + D_1\left[\mathrm{e}^{D_2\left(\bar{I}_1 - 3\right)} - 1\right] + \xi\left(J - 1\right) \quad (1)$$

in which $\bar{I}_1 = J^{-2/3}I_1$; I_1 is the first invariant of the unimodular component of the left Cauchy-Green deformation tensor; J is the determinant of the deformation gradient; ξ is the Lagrangian multiplier for the assumption of incompressibility; C_1, D_1 and D_2 are the empirical material constants to be determined by

experimental data. In the case of uni-axial tensile experiment, the Cauchy stress σ_{11} along the tensile direction is derived as,

$$\sigma_{11}(\lambda) = 2\left(\lambda^2 - \frac{1}{\lambda}\right)\left[C_1 + D_1 D_2 e^{D_2\left(\lambda^2 + \frac{2}{\lambda} - 3\right)}\right] \quad (2)$$

in which λ is the stretch ratio.

C. Ordinary Least Square Fitting Method

The ordinary least square (OLS) [19] fitting method was used to determine the material constants in Eq. (1) by finding the local minimum of the objective function around the initial guess of (C_{10}, D_{10}, D_{20}),

$$S(C_1, D_1, D_2) = \sum_{k=1}^{N}\left[\sigma_{11k}^P - \sigma_{11k}^M\right]^2 \quad (3)$$

in which N is the number of data points, σ_{11k}^P and σ_{11k}^M are the kth predicted and measured Cauchy stresses, respectively. All material constants were constrained to be positive to avoid any unphysical phenomenon. Relative error was used to assess the fitting quality [20],

$$\gamma = \frac{\sum_{i=k}^{N}\left|\sigma_{11k}^P - \sigma_{11k}^M\right|}{\sum_{i=k}^{N}\left|\sigma_{11k}^M\right|} \times 100\% \quad (4)$$

D. Bayesian Inference Framework

In the Bayesian inference, all unknown parameters are treated as random variables $\boldsymbol{\theta}$. Given the experimental data $\mathcal{D}$, its aim is to estimate the conditional distribution of unknown parameters $p(\boldsymbol{\theta}|\mathcal{D})$, which is referred to the posterior distribution (*posterior*). First a prior distribution (*prior*) $p(\boldsymbol{\theta})$ is assumed to represent the prior knowledge about unknown parameters. The prior distribution can be adapted from previous studies and/or from experts' opinions. If there is no established prior distribution for a problem, a non-informative *prior* can be applied using the Principle of Maximal Entropy.

An appropriate noise model and chosen constitutive equations are used to derive the likelihood function (*likelihood*) $p(\mathcal{D}|\boldsymbol{\theta})$. The *posterior* can be calculated by linking the *prior* and the *likelihood* using Bayes' theorem [21]–[23],

$$p(\boldsymbol{\theta}|\mathcal{D}) = \frac{p(\boldsymbol{\theta}) \times p(\mathcal{D}|\boldsymbol{\theta})}{p(\mathcal{D})} \quad (5)$$

The denominator of Eq. (5) is a constant referred to as the probability of the evidence (*evidence*) and given by,

$$p(\mathcal{D}) = \int p(\boldsymbol{\theta}) \times p(\mathcal{D}|\boldsymbol{\theta}) \, d\boldsymbol{\theta} \quad (6)$$

The multi-dimensional integral in Eq. (6) is generally difficult to evaluate. If the unknown parameters are the only ones of interest, Eq. (6) can be rewritten as [21]–[23],

$$p(\boldsymbol{\theta}|\mathcal{D}) \propto p(\boldsymbol{\theta}) \times p(\mathcal{D}|\boldsymbol{\theta}) \quad (7)$$

Sampling methods, e.g., Markov Chain Monte Carlo (MCMC), can be applied to explore the *posterior* without explicitly computing the *evidence* (Eq. (6)). The strategy is to draw samples from a distribution similar to the *posterior* by using effective sampling methods. More details about Bayesian inference and different sampling methods can be found in references [21]–[23].

When Bayesian inference is used to estimate the material constants in Eq. (1), a Gaussian noise model [21]–[23] is introduced for the uncertainty, hoping that $\sigma_{11k}^P(\lambda)$ equals to $\sigma_{11k}^M(\lambda)$

$$\sigma_{11}(\lambda) = 2\left(\lambda^2 - \frac{1}{\lambda}\right)\left[C_1 + D_1 D_2 e^{D_2\left(\lambda^2 + \frac{2}{\lambda} - 3\right)}\right]$$
$$+ \mathcal{N}\left(0, \varepsilon^2\right) \quad (8)$$

where, $\mathcal{N}(0, \varepsilon^2)$ is the additive Gaussian noise with zero mean and variance ε^2 (standard deviation ε). Therefore, the likelihood function can be written as,

$$p(\mathcal{D}|C_1, D_1, D_2, \varepsilon) = \prod_{k=1}^{N} \mathcal{N}\left(\sigma_{11k}^P - \sigma_{11k}^M | 0, \varepsilon^2\right) \quad (9)$$

where N is the number of experimental data points. In this study, the *prior* for C_1, D_1, D_2 and ε were assumed to be uniform distributions with ranges of [0, 5000] kPa, [0, 5000] kPa, [0, 5000] and [0, 5000] kPa, respectively. The sensitivity to the *prior* was tested. The MCMC with Gibbs sampling method was implemented in the software WinBUGS (MRC Biostatistics Unit, University of Cambridge) to estimate the posterior distribution of the parameters, i.e., $p(\boldsymbol{\theta}|\mathcal{D})$. The mean and standard deviation of the *posterior* was calculated for further analyses amongst tissues from different types of lesions and distinct morphological component.

E. Quantitative Histological Analysis

Twenty four tissue strips adjacent to those used for mechanical testing from the 8 aneurysmal samples (3 strips from each sample), which were collected from Papworth Hospital were submitted for histological examination. Following a standard histological processing procedure, tissue slices in 4 μm thickness were stained with Elastin Van Gieson (EVG) and Sirius Red to visualise the elastin and collagen contents, respectively. Stained histological tissue slices were digitised with the NanoZoomer Slide Imaging System (Hamamatsu, Hamamatsu City, Japan) at the amplification rate of 40 into 904 nm resolution RGB images. Elastin appears dark in EVG stain, and collagen appears red in Sirius Red stain. Elastin and collagen percentage of each tissue slice, as well as the fibre dispersion (κ; a parameter describing the scatter of fibre orientations), and fibre waviness (ω) were quantified using an in-house designed MATLAB-based (MathWorks, Inc.) software as described in the **Supplementary Material**. The software was optimised with the help of a pathology expert who had more than 15 years of experience in histopathological analysis of diseased arterial tissues.

In this study, the area percentage of elastin (= area with elastin/area of ROI, ROI stands for region of interest) and collagen (= area with collagen/area of ROI), κ, and ω were used to characterize the fibre architecture in the structure. Perfectly parallel fibres correspond to $\kappa = 0$ and an even scatter of fibre orientations has $\kappa = 1/3$. Smaller values of ω correspond to straighter fibres, and $\omega = 0$ indicates straight fibres.
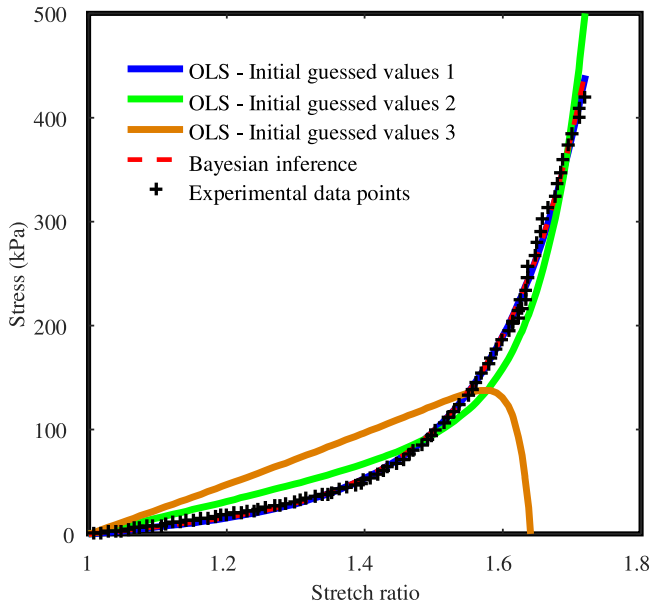
Fig. 1. A representative example showing the fitted results using ordinary least square (OLS) method and Bayesian inference (initially guessed values 1 of (C_1, D_1, D_2) are (1, 1, 1), values 2 are (10, 10, 10), and values 3 are (100, 100, 100); the detailed fitted results are listed in Table I; the experimental data were acquired from a media strip of a normal aorta).

F. Statistical Analysis

The correlation between the percentage of collagens and the estimated material constants was assessed using Spearman correlation test. In this study, multiple samples were collected from each tissue piece and the linear mixed effect model was constructed to assess the difference of parameters from different tissue types, considering both random and fixed effects. The statistical analysis was performed in MATLAB (MathWorks, Inc.). A significant difference was assumed if $p < 0.05$.

III. RESULTS

In this study, stress-stretch curves from 312 tissue strips in the circumferential direction (perpendicular to the direction of blood flow) were analysed using both OLS and Bayesian inference (Fig. 1).

In detail, the curves were from 15 media and 15 adventitial strips of 8 normal aortas; 28 adventitial, 36 media, 8 thickened intima and 27 thrombus strips of 19 aortic aneurysms; 65 media, 59 fibrous cap (FC), 38 lipid, and 21 intraplaque haemorrhage/thrombus (IPH/T) strips of 21 carotid atherosclerotic plaques. The difference in material constants determined by Bayesian inference of different tissue types was explored (Fig. 2) and the association between determined constants and tissue micro architectures was investigated (Figs. 3 and 4).

A. Case Study on Material Constants' Uniformity

Fig. 1 provides a representative example showing the fitted results using OLS fitting method and Bayesian inference. The determined material constants were dependent on initial
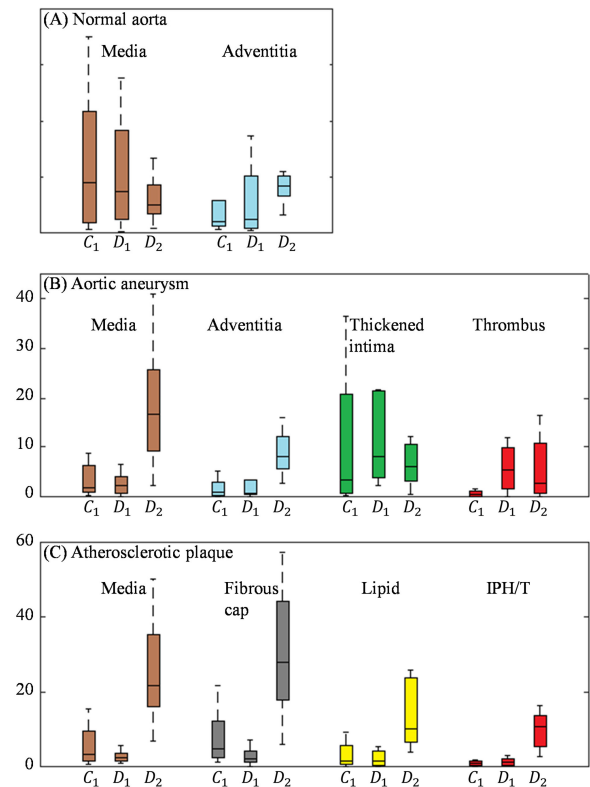

Fig. 2. The visualization of (C_1, D_1, D_2) of different tissue strips from different types of samples. (a) Tissue strips of media and adventitia from normal aortas. (b) Tissue strips of media, adventitia, thickened intima, and thrombus from aortic aneurysms. (c) Tissues strips of media, fibrous cap, lipid, and intraplaque haemorrhage/thrombus from carotid atherosclerotic plaques. Unit of C_1 and D_1 is kPa and D_2 is dimensionless.

guesses when OLS method was used. In the cases shown in Fig. 1, when the initial guesses of (1, 1, 1) and (10, 10, 10) were used, the fitting results were very different (Table I). A certain choice of initial guesses, e.g., (100, 100, 100), might lead to a poor regression (Fig. 1). It is therefore inappropriate to use material constants determined by OLS to characterise the mechanical properties of arterial tissues. On the contrary, based on Bayesian inference, the determined material constants showed little changes ($<5\%$) when the *prior* ranges of C_1, D_1 and D_2 all increased ten times from [0, 1000] to [0, 10000].

In general, if the initially guessed value is properly chosen, OLS can fit the experimental data well. The fitting quality γ was 8.5% [6.0, 12.1] (Median [Interquartile range]), which is slightly better than that of the Bayesian inference-based estimation (8.8% [6.0, 12.3], $p < 0.0001$).

B. Bayesian Inference-Based Material Constants of Different Tissues Types

The values of C_1, D_1 and D_2 for each type of tissue are provided in Fig. 2 (the outliers that are out of 1.75 quartile range were not shown) with actual values listed in Table II. In normal aorta, the media and adventitia have comparable C_1, D_1 and D_2 ($p = 0.18$, 0.33, and 0.14, respectively). Samples from the aortic aneurysm, media and thickened intima showed
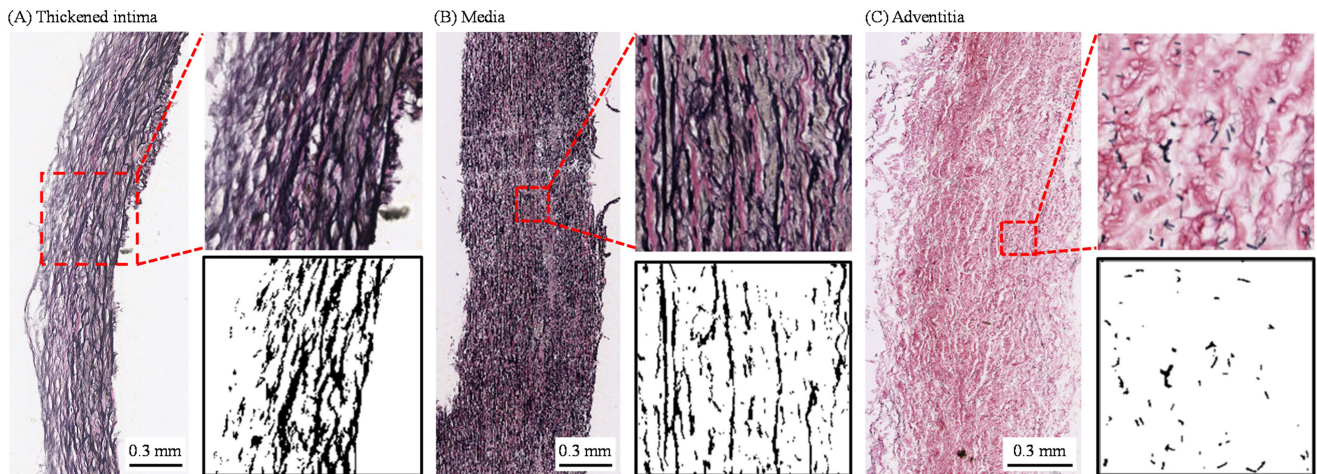
Fig. 3. Representative EVG stained images showing the distribution of elastin in dark in the thickened intima, media, and adventitia of an aortic aneurysm (The elastin contents are segmented in black. Adventitia has much less elastin fibres than either thickened intima or media). (a) Thickened intima. (b) Media. (c) Adventitia.

TABLE I
REPRESENTATIVE REGRESSIONS USING THE ORDINARY LEAST SQUARE (OLS) METHOD WITH DIFFERENT INITIAL VALUES AND BAYESIAN INFERENCE PROCEDURE WITH DIFFERENT *prior* RANGES

Fitting Method	C_1 (kPa)	D_1 (kPa)	D_2	γ
OLS - Initial values (1, 1, 1)	2.19	4.00	2.12	3.3%
OLS - Initial values (10, 10, 10)	25.56	0.04	5.27	15.1%
OLS - Initial values (100, 100, 100)	39.10	2.65×10^{-8}	19.92	444.5%
OLS - Initial values (0, 1, 0)	6.17	2.84	2.31	3.1%
Bayesian inference (*Prior* [0, 1000])	3.11	3.72	2.16	3.3%
Bayesian inference (*Prior* [0, 5000])	3.26	3.67	2.17	3.3%
Bayesian inference (*Prior* [0, 10000])	3.20	3.68	2.17	3.3%

TABLE II
BAYESIAN INFERENCE-BASED ESTIMATIONS FOR DIFFERENT TYPES OF TISSUES (MEDIAN [INTERQUARTILE RANGE])

|		C_1 (kPa)	D_1 (kPa)	D_2	γ (%)
Normal aorta	Media	4.53 [0.88, 10.84]	3.68 [1.19, 9.21]	2.53 [1.74, 4.29]	3.3 [2.3, 4.5]
	Adventitia	1.04 [0.60, 3.46]	1.46 [0.75, 6.51]	3.57 [3.12, 5.26]	9.8 [5.5, 13.6]
Aneurysm	Media	1.81 [0.83, 6.31]	2.33 [0.79, 4.02]	16.77 [9.12, 25.71]	11.8 [8.8, 14.7]
	Adventitia	0.96 [0.30, 2.88]	0.79 [0.56, 3.40]	8.04 [5.60, 12.13]	12.0 [7.2, 14.8]
	Intima	3.27 [0.74, 20.91]	7.98 [3.82, 21.42]	6.05 [3.04, 10.44]	7.9 [5.6, 11.5]
	Thrombus	0.46 [0.12, 1.17]	5.34 [1.66, 9.90]	2.80 [0.59, 10.77]	8.3 [7.2, 14.1]
Atherosclerosis	Media	3.34 [1.44, 9.60]	2.27 [1.45, 3.62]	21.78 [16.16, 35.24]	7.7 [6.6, 9.6]
	FC	4.87 [2.50, 12.33]	2.21 [1.26, 4.16]	28.06 [17.95, 44.17]	9.2 [7.0, 11.5]
	Lipid	1.48 [0.71, 5.62]	1.40 [0.28, 4.15]	10.07 [6.42, 23.66]	8.4 [5.9, 11.4]
	IPH/T	0.79 [0.18, 1.47]	1.17 [0.44, 2.20]	10.58 [5.45, 13.63]	10.8 [8.2, 18.4]
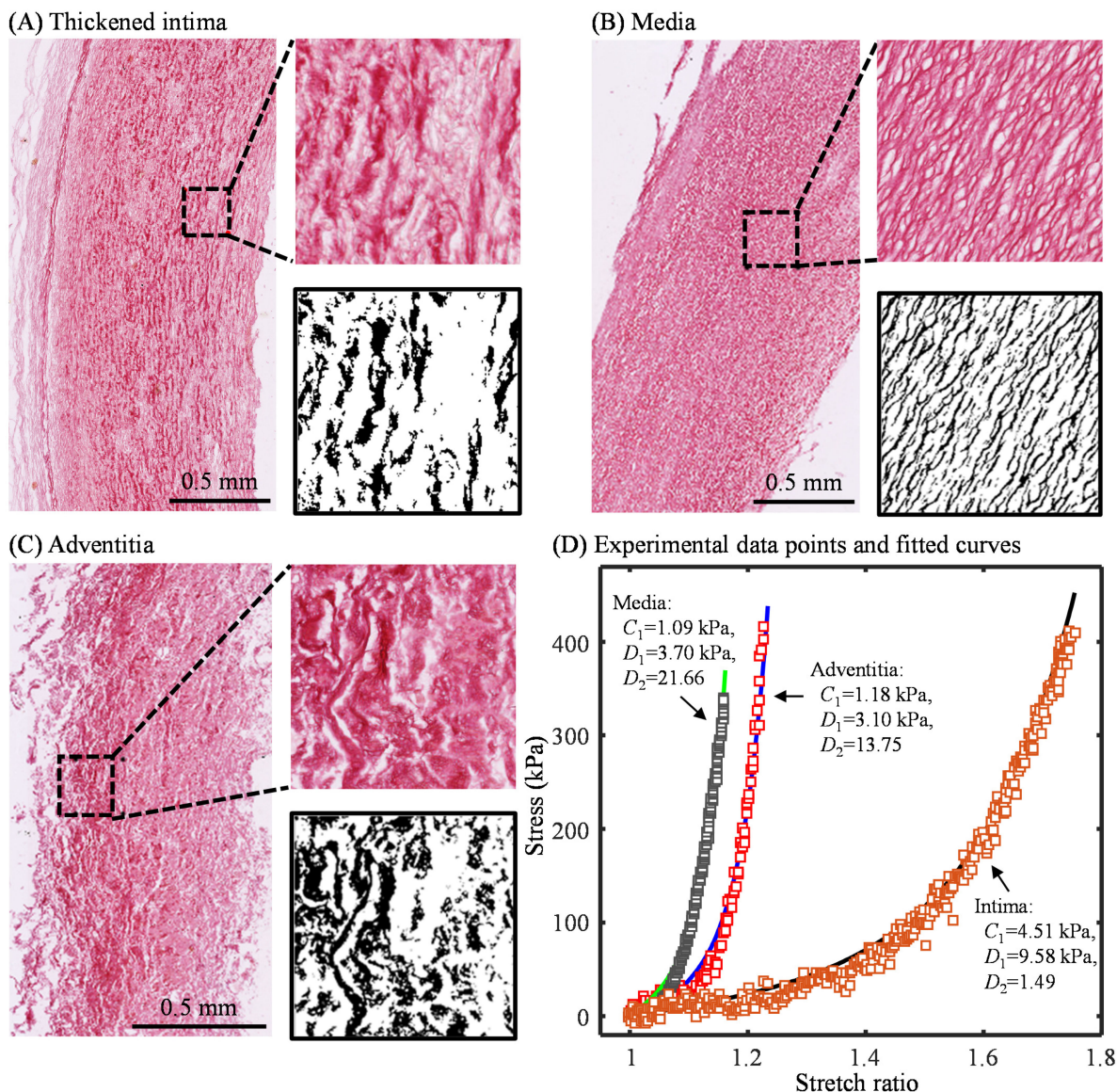
Fig. 4. Representative Sirius Red stained images showing the collagen fibres in red in the thickened intima, media, and adventitia of an aortic aneurysm (The collagen contents are segmented in black. Collagen fibres in the adventitia (C) is much wavier than those in the media (B). D: the stress-stretch curves of the tissue strips are shown in (A–C). More extensible tissues have smaller D_2). (A) Thickened intima. (B) Media. (C) Adventitia. (D) Experimental data points and fitted curves.

a comparable C_1 ($p = 0.50$), which is significantly higher than that in either adventitia or thrombus ($p<0.05$). Adventitia has the lowest value of D_1 ($p<0.005$); intima has the highest value of D_1 ($p<0.01$) but is comparable with the one of thrombus ($p = 0.21$). Media has the highest D_2 value compared with adventitia, thickened intima and thrombus ($p<0.05$); and thrombus has the lowest value of D_2 ($p<0.05$) but is comparable with that of intima ($p = 0.29$).

In carotid atherosclerosis, media and FC have a comparable C_1 ($p = 0.33$), significantly higher than those of lipid and IPH/T ($p<0.05$). Compared with IPH/T, C_1 value of lipid is significantly higher ($p = 0.03$). The value of D_1 for media, FC and lipid is comparable ($p>0.05$), and IPH/T has the lowest value of D_1 compared with media and FC ($p<0.01$) but is comparable with that of lipid ($p = 0.87$). Both media and FC have a

comparable D_2 ($p = 0.33$), as do lipid and IPH/T ($p = 0.39$); both media and FC have a significantly higher D_2 than either lipid or IPH/T ($p<0.005$).

Media is the only common tissue type in normal aorta, aortic aneurysm and atherosclerotic plaque. Only material constants of media of these three types of tissue were therefore compared. The C_1 value of media from normal aorta, aortic aneurysm and carotid atherosclerotic plaque is comparable ($p>0.05$), as is D_1 ($p>0.05$). However, D_2 has the capacity to differentiate all three types of tissues. In general, smaller values of D_2 correspond to more extensible tissues (Fig. 4(d)). The value of D_2 for the media from both aneurysm and plaque is significantly larger than that from normal aorta ($p<0.0001$), and the D_2 value of media from plaque is much larger than that from aneurysm ($p = 0.022$).
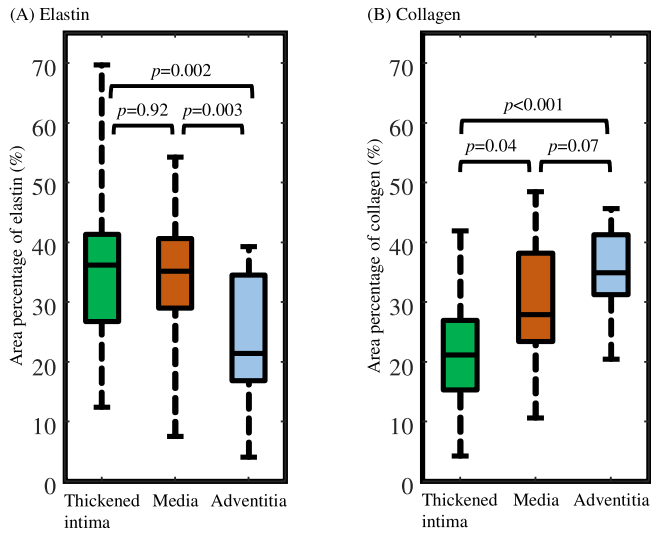
Fig. 5. Comparison of area percentage of elastin and collagen contents in the thickened intima, media, and adventitia from eight aortic aneurysms. (a) Elastin. (b) Collagen.

Fig. 6. The association between collagen fibre dispersion (κ) and waviness (ω) and D_2. (a) Dispersion. (b) Waviness.

C. Material Constants, Elastin and Collagen Contents and Architectures

One tissue strip adjacent to the one for mechanical testing of each layer from each of the eight aneurysm samples from Papworth Hospital were submitted for histological examination to visualise the elastin and collagen in the tissue microstructure (Figs. 3 and 4).

As shown in Fig. 5(a), the area percentage of elastin in both thickened intima and media is higher than the adventitia (an example is shown in Fig. 3), and thickened intima has the lowest area percentage of collagen (Fig. 5(b)), followed by media, where the adventitia has the highest area percentage of collagen (an example is shown in Fig. 4). The difference in elastin content in these three layers (Fig. 5(a)) is consistent with the difference of C_1 value as listed in Table II.

Elastin fibres in the thickened intima and media are mostly well organised and straight while those in the adventitia are more fragmented (Fig. 3). Similarly, the collagen fibres in the thickened intima and media are straight with a preferred direction, while in the adventitia the collagen fibres are wavier and more disorganised. Compared with the media, the collagen fibre dispersion, κ, is much bigger (0.14 [0.13, 0.15] vs 0.23 [0.19, 0.25], $p = 0.008$), and the waviness, ω, is higher in adventitia (0.07 [0.09, 0.12] vs 0.16 [0.15, 0.18], $p = 0.008$). When κ, ω, D_1 and D_2 of media and adventitia were pooled, κ was inversely associated with D_2 ($\rho = -0.61$, $p = 0.014$) and ω was inversely associated with D_2 ($\rho = -0.73$, $p = 0.002$) (Fig. 6); but no association was found between D_1 and κ or ω.

IV. DISCUSSION

Bayesian inference estimates the distribution of material parameters in the constitutive model rather than finding their point-based estimations. It is used in this study to avoid the sensitivit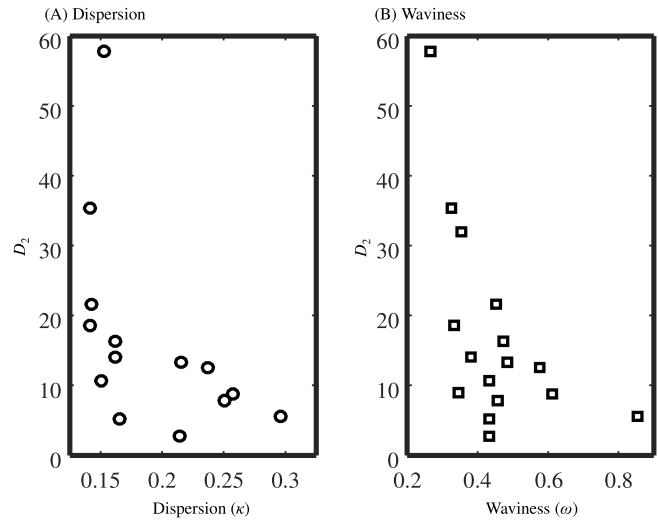y to initial guesses when OLS method is used, allowing characterisation of the tissue through comparison of material constants. Obtained results indicated that C_1, D_1 and D_2 were tissue type dependent. In particular, D_2 is the most sensitive parameter in differentiating tissues of distinct arterial layers from a single type of sample, or of the same layer between different type of samples; and D_2 is also associated with tissue architectures, e.g., fibre dispersion and waviness. In general, atherosclerotic tissues have the biggest D_2 values, followed by those from aneurysms and then normal aortas.

Proper choice of both SEDF and material constants is important for material stability and numerical convergence in computational studies that aim to predict stress distribution within the lesion [17], [24]. The robustness of the SEDF is reflected by its ability to reproduce several modes of deformation, including, but not limited to uni-axial, bi-axial and pure shear deformations [17]. Considering its stability and broad capacity in characterizing distinct material properties, the modified Mooney-Rivlin SEDF appear as practical choice for mechanical analyses to predict the critical mechanical conditions within vascular lesions, such as carotid atherosclerotic plaques [17]. In this study, stress-stretch data from uni-axial testing was used, since it is nearly impossible to perform bi-axial and pure shear testing with atherosclerotic tissues, because of their non-homogeneity and irregularity. Regarding material constants of the SEDF, using constraints on their values can make the SEDF convex to achieve material stability to a particular extent [25]. Although a wide search with multiple initial guesses might alleviate the sensitivity of material constants to the initial guess, an exhausted try is not possible and moreover, different sets of material constants may all have a satisfactory regression, e.g., with a small γ value. However, this does not imply the uniqueness of OLS in material constants identification as Bayesian approach does in a large space. For example, the initial guesses of (1, 1, 1) and (0, 1, 0) can both fit the experimental data points shown in Fig. 1 well, but with very different material constants, in particular, C_1 and D_1 (Table I).

TABLE III
COMPARISON OF MATERIAL CONSTANT DETERMINATION METHODS (RESULTS ARE PRESENTED IN MEAN ± SD)

| Noise (kPa)	Methods for the determination of material constants	C_1 (kPa)	D_1 (kPa)	D_2	γ (%)
0	OLS - Initial values (0, 1, 0)	1.19	4.36	2.06	0.60
	OLS - Initial values (1, 1, 1)	3.26	3.67	2.16	0.00
	OLS with MultiStart Algorithm	3.26	3.67	2.16	0.00
	Bayesian inference	3.25	3.67	2.16	0.10
1	OLS - Initial values (0, 1, 0)	1.64±0.86	4.22±0.30	2.08±0.04	1.0±0.1
	OLS - Initial values (1, 1, 1)	3.35±0.48	3.65±0.16	2.16±0.02	0.9±0.1
	OLS with MultiStart Algorithm	3.36±0.47	3.65±0.15	2.16±0.02	0.9±0.1
	Bayesian inference	3.32±0.48	3.67±0.16	2.16±0.03	0.9±0.1
5	OLS - Initial values (0, 1, 0)	1.57±1.75	4.30±0.60	2.08±0.10	4.6±0.5
	OLS - Initial values (1, 1, 1)	3.71±2.28	3.62±0.73	2.18±0.12	4.5±0.5
	OLS with MultiStart Algorithm	3.71±2.28	3.62±0.74	2.18±0.12	4.5±0.5
	Bayesian inference	3.56±1.65	3.66±0.54	2.18±0.10	4.9±0.7
10	OLS - Initial values (0, 1, 0)	1.71±2.70	4.37±1.00	2.08±0.18	9.0±1.0
	OLS - Initial values (1, 1, 1)	4.41±3.90	3.54±1.23	2.22±0.23	9.0±1.1
	OLS with MultiStart Algorithm	4.41±3.90	3.54±1.23	2.22±0.23	9.0±1.1
	Bayesian inference	4.20±2.32	3.59± 0.73	2.20±0.15	9.8±1.5
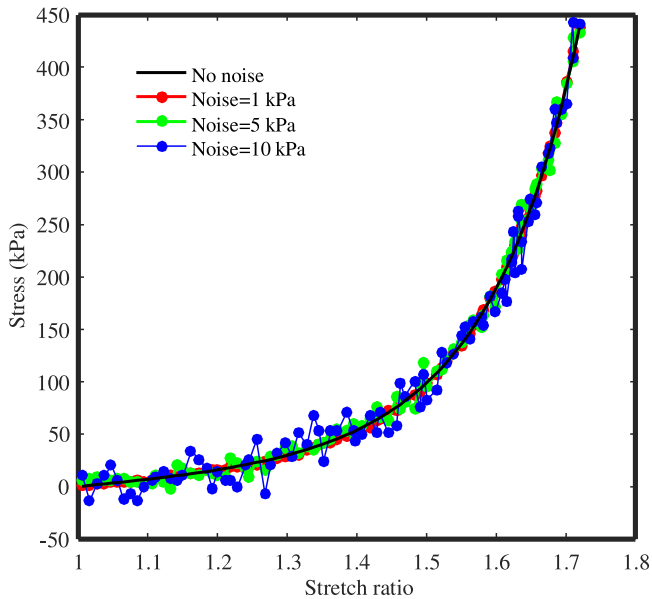
Fig. 7. Representative curves with Gaussian noise and with different standard deviations (The template curve was generated with $C_1 = 3.26$ kPa, $D_1 = 3.67$ kPa, and $D_2 = 2.16$).

The employment of Bayesian inference-based approach can eliminate such dependencies. It provides an estimation of the distribution of the parameters instead of a point estimation. The expectation of the distribution is used as the determined material constant which provides the uniqueness, in particular for noisy data (please refer to Fig. 7 and Table III and associated discussion in the paragraph below for details).

The non-uniqueness of parameter estimation associated with OLS might be avoided with a hybrid approach by searching different initial guesses aiming at a global minimisation within a large space. MultiStart Algorithm [26] implemented in Global Optimization Toolbox of MATLAB (MathWorks, Inc.) was used to follow this principle. A parameter study was performed to compare the difference between this and Bayesian inference-based approaches. A standard stretch-stress curve was generated using $C_1 = 3.26$ kPa, $D_1 = 3.67$ kPa, $D_2 = 2.16$ that fit the experimental data shown in Fig. 1. Gaussian noise with three different standard deviations ($\varepsilon = 1, 5$ and 10 kPa) was added to the curve (Fig. 7) and the noising process was repeated independently for 1000 times for each σ to generate 1000 artificial curves. OLS with initial guesses of (0, 1, 0) and (1, 1, 1), OLS with MultiStart Algorithm and Bayesian inference-based approach were used to identify the constants as listed in Table III. In the case of no noise, the OLS method with initial guess (0, 1, 0) found a local minimum, where the fitted results did not match the gold standard well. The OLS method with (1, 1, 1) achieved equally good fitting results compared to OLS method with global minimisation algorithm, indicating (1, 1, 1) is a good initial guess. The Bayesian method found approximately the same parameters, with a gamma value of 0.1%. For all approaches, the shifting mean value of constants and increased γ at higher noise levels were found. Bayesian method obtained similar mean values and standard deviations to the OLS method with global minimization, although when the noise level increased to 5 kPa and higher, Bayesian inference-based approach performed slightly better with a closer mean value to the gold standard and smaller standard deviation. It can be expected that its performance could be further improved with an appropriate *prior*. Other

sophisticated minimization algorithms, e.g., genetic algorithm [27], are also available to achieve a global optimum within a large space to avoid non-uniqueness in material parameters identification.

The material constants, C_1, D_1 and D_2 contribute differently to the stress when the tissue strip is subject to stretching as shown in Eq. (2). Taking the results in Fig. 1 as an example, when $\lambda = 1.2$, the term with C_1 contributes 21.2% to the total stress and the term with D_1 and D_2 contributes the rest; when $\lambda = 1.6$, the proportion from the term with C_1 decreases to 6.3%, and that from D_1 and D_2 increases to 93.7%. In general, the change in curve is insensitive to the change of C_1, more prominent with changes in D_1, and very profound with changes in D_2 (Please see **Supplementary Material** for more details).

The extracellular matrix components, specifically the mix of elastin and collagen in the vessel wall, determine the passive mechanical properties of large arteries. C_1, D_1 and D_2 might be used to characterise their mechanical behaviour under physiological and pathological conditions. In an unloaded healthy artery, both elastin and collagen appear undulated and wavy, where they straighten as the artery begins to bear load [28]. The elastin is mostly straight at physiological pressures [28]. Upon involvement of C_1, the term in Eqs. (1) and (2) may reflect this procedure. In contrast to the elastin, less than 10% of the collagen fibres are straight and load-bearing at physiological pressures [29]. As the pressure increases, more collagen fibres become load-bearing and their stiffness limits arterial distension, providing the classical nonlinear behaviour observed in arterial mechanics [30]. This is characterised by the term in Eqs. (1) and (2) with D_1 and D_2 involvement, particularly, D_2 dominates the rate of increase in stress. Elastin and collagen fibres can be degraded by several members of the matrix metalloproteinase (MMP) family. Increased expression of MMP-1 and MMP-9, for example, have been reported in aneurysms, which are characterized by fragmentation of both elastin and collagen fibres [31], where the increased expression of MMP-2 is localized to sites of fragmentation in the elastic lamellae [32]. These pathological changes lead to a stiffer artery, that is, stress increases quicker during stretching. The bigger D_2 value of aneurysmal and atherosclerotic tissues can be the consequence of these pathological changes.

It is worth noting that the modified Mooney-Rivlin SEDF is a phenomenological approximation of the material behaviour. Information from microstructure was not used, and therefore material parameters C_1, D_1 and D_2 can only loosely link to the fibre architecture. Moreover, the exponential term describing the toe region in the stress-stretch curve is oversimplified and unbounded, allowing the tangential stiffness to rise infinitely with increasing stretch. Such limitations can be overcome by employing a more microstructurally informed model, which takes gradual recruitment of collagen fibres into consideration [33]–[35]. In their stress-free state, the collagen fibres rest in a crimped configuration with waviness following a right-skewed distribution [36], [37]. As a result, the likelihood of collagen fibres becoming newly recruited follows a Gamma distribution,

$$\Gamma\left(\bar{I}_1; \alpha, \beta\right) = \frac{\beta^\alpha \left(\bar{I}_1 - 3\right)^{\alpha-1} e^{-\beta\left(\bar{I}_1 - 3\right)}}{\Gamma\left(\alpha\right)} \qquad (10)$$

where Γ_α is a complete Gamma function, and α and β are the shape and rate parameters. Both parameters relate to the microstructure of the tissue, with $\alpha\beta^{-1}$ and $\alpha\beta^{-2}$ being the expectation and variance of $\bar{I}_1 - 3$ at which the collagen fibres become recruited. Integrating this probability density function gives the cumulative likelihood of collagen fibres contributing to stiffness. Thus, SEDF at a given stretch level can be obtained as follows,

$$W = C_1\left(\bar{I}_1 - 3\right) + D_1 \int_0^{\bar{I}_1} \Gamma\left(x; \alpha, \beta\right) dx \qquad (11)$$

where C_1 and D_1 reflect the contribution (incorporating fibre stiffness, alignment and relative volume fraction) of elastin and collagen fibres, respectively. Such a formulation offers more flexibility in fitting and better insights in the mechanical response [34], [35], however the whole fitting procedure is much more complicated than either OLS or Bayesian inference-based estimation. Given that phenomenological models already lead to comparable goodness of fit [34], we conducted the present study using modified Mooney-Rivlin models for conciseness.

It is necessary to disclose that the experimental data used in this study were mostly from two previous reports [16], [18]. The non-uniqueness in the material constants identification using OLS was mentioned in one of them [16]. To obtain a determined set of material constants for each type of tissue, an energy-based average algorithm was employed. It is certain that the findings and conclusions obtained in this study do not relate to any of these two previous reports.

The obtained estimations listed in Table II can serve as *priors* for future studies to improve the accuracy of the estimation. Despite the interesting findings, limitations exist in this study: (1) the stress-stretch curve used in this study was from uni-axial tests and modified Mooney-Rivlin SEDF is an isotropic model, so that the anisotropy was not considered. The anisotropic SEDF considering microstructures can be found in studies by Holzapfel *et al.* [38]; (2) EVG and Sirius Red stains were used to visualise the gross elastin and collagen architectures and pathological features, e.g., inflammation, was not considered that might affect tissue mechanical properties and therefore the value of C_1, D_1 and D_2; and (3) modified Mooney-Rivlin SEDF usually can fit the whole stress-stretch curve of the normal aorta well, but not for all tissue strips of aneurysm and atherosclerotic plaque, in particular, in the region with a low stretch level (Fig. 4(d)).

REFERENCES

[1] WHO, "World Health Statistics 2017: Monitoring health for the SDGs, Sustainable Development Goals," Villars-sous-Yens, Switzerland, 2017.

[2] I. M. Nordon *et al.*, "Pathophysiology and epidemiology of abdominal aortic aneurysms," *Nat. Rev. Cardiol.*, vol. 8, pp. 92–102, 2011.

[3] W. H. Pearce *et al.*, "Atherosclerotic peripheral vascular disease symposium II: Controversies in abdominal aortic aneurysm repair," *Circulation*, vol. 118, pp. 2860–2863, 2008.

[4] C. North American Symptomatic Carotid Endarterectomy Trial, "Beneficial effect of carotid endarterectomy in symptomatic patients with high-grade carotid stenosis," *N. Engl. J. Med.*, vol. 325, pp. 445–453, 1991.

[5] F. A. Lederle *et al.*, "Immediate repair compared with surveillance of small abdominal aortic aneurysms," *N. Engl. J. Med.*, vol. 346, pp. 1437–1444, 2002.

[6] S. C. Nicholls *et al.*, "Rupture in small abdominal aortic aneurysms," *J. Vasc. Surg.*, vol. 28, pp. 884–888, 1998.

[7] J. T. Powell *et al.*, "The rupture rate of large abdominal aortic aneurysms: Is this modified by anatomical suitability for endovascular repair?," *Ann. Surg.*, vol. 247, pp. 173–179, 2008.

[8] K. Asanuma *et al.*, "Uniaxial strain upregulates matrix-degrading enzymes produced by human vascular smooth muscle cells," *Am. J. Physiol. Heart Circ. Physiol.*, vol. 284, pp. H1778–H1784, 2003.

[9] S. R. Vallabhaneni *et al.*, "Heterogeneity of tensile strength and matrix metalloproteinase activity in the wall of abdominal aortic aneurysms," *J. Endovasc. Ther.*, vol. 11, pp. 494–502, 2004.

[10] N. von Offenberg Sweeney *et al.*, "Cyclic strain-mediated regulation of endothelial matrix metalloproteinase-2 expression and activity," *Cardiovasc. Res.*, vol. 63, pp. 625–634, 2004.

[11] A. Maier *et al.*, "Correlation of biomechanics to tissue reaction in aortic aneurysms assessed by finite elements and [18F]-fluorodeoxyglucose-PET/CT," *Int. J. Numer. Method Biomed. Eng.*, vol. 28, pp. 456–471, 2012.

[12] Y. Huang *et al.*, "High structural stress and presence of intraluminal thrombus predict abdominal aortic aneurysm 18F-FDG Uptake: Insights from biomechanics," *Circ. Cardiovasc Imaging*, vol. 9, 2016, Art. no. e004656.

[13] R. R. F. Stevens *et al.*, "Biomechanical changes during abdominal aortic aneurysm growth," *PLoS One*, vol. 12, 2017, Art. no. e0187421.

[14] V. Thondapu *et al.*, "Biomechanical stress in coronary atherosclerosis: emerging insights from computational modelling," *Eur. Heart J.*, vol. 38, pp. 81–92, 2017.

[15] A. Tuenter *et al.*, "High shear stress relates to intraplaque haemorrhage in asymptomatic carotid plaques," *Atherosclerosis*, vol. 251, pp. 348–354, 2016.

[16] Z. Teng *et al.*, "Material properties of components in human carotid atherosclerotic plaques: a uniaxial extension study," *Acta Biomater.*, vol. 10, pp. 5055–5063, 2014.

[17] Z. Teng *et al.*, "The influence of constitutive law choice used to characterise atherosclerotic tissue material properties on computing stress values in human carotid plaques," *J. Biomech.*, vol. 48, pp. 3912–3921, 2015.

[18] Z. Teng *et al.*, "Layer- and direction-specific material properties, extreme extensibility and ultimate material strength of human abdominal aorta and aneurysm: A uniaxial extension study," *Ann. Biomed. Eng.*, vol. 43, pp. 2745–2759, 2015.

[19] F. Galton, "Regression towards mediocrity in hereditary stature," *J. Anthropological Inst. Great Britain Ireland*, vol. 15, pp. 246–263, 1886.

[20] N. R. Farnum, "Improving the relative error of estimation," *Amer. Statist.*, vol. 44, pp. 288–289, 1990.

[21] S. Madireddy *et al.*, "A Bayesian approach to selecting hyperelastic constitutive models of soft tissue," *Comput. Methods Appl. Mech. Eng.*, vol. 291, pp. 102–122, 2015.

[22] S. Madireddy *et al.*, "Bayesian calibration of hyperelastic constitutive models of soft tissue," *J. Mech. Behavior Biomed. Mater.*, vol. 59, pp. 108–127, 2016.

[23] S. Doraiswamy *et al.*, "A technique for the classification of tissues by combining mechanics based models with Bayesian inference," *Int. J. Eng. Sci.*, vol. 106, pp. 95–109, 2016.

[24] Adina, *Instability of Two-Term Mooney-Rivlin Model.* May 2009. [Online]. Available: http://www.adina.com/newsgH48.shtml

[25] R. W. Ogden, *Nonlinear Elasticity, Anisotropy, Material Stability and Residual Stresses in Soft Tissue.* Udine, Italy: Springer-Verlag, 2003.

[26] Z. Ugray *et al.*, "Scatter search and local NLP Solvers: A multistart framework for global optimization," *INFORMS J. Comput.*, vol. 19, pp. 328–340, 2007.

[27] B. M. Chaparro *et al.*, "Material parameters identification: Gradient-based, genetic and hybrid optimization algorithms," *Comput. Mater. Sci.*, vol. 44, pp. 339–346, 2008.

[28] J. M. Clark and S. Glagov, "Transmural organization of the arterial media. The lamellar unit revisited," *Arteriosclerosis*, vol. 5, pp. 19–34, 1985.

[29] R. L. Armentano *et al.*, "Assessment of elastin and collagen contribution to aortic elasticity in conscious dogs," *Amer. J. Physiol.*, vol. 260, pp. H1870–H1877, 1991.

[30] H. Wolinsky and S. Glagov, "Structural basis for the static mechanical properties of the aortic media," *Circ. Res.*, vol. 14, pp. 400–413, 1964.

[31] N. A. Tamarina *et al.*, "Expression of matrix metalloproteinases and their inhibitors in aneurysms and normal aorta," *Surgery*, vol. 122, pp. 264–271, 1997.

[32] Z. Li *et al.*, "Increased expression of matrix metalloproteinase-2 in the thickened intima of aged rats," *Hypertension*, vol. 33, pp. 116–23, 1999.

[33] A. J. Bank *et al.*, "Contribution of collagen, elastin, and smooth muscle to in vivo human brachial artery wall stress and elastic modulus," *Circulation*, vol. 94, pp. 3263–3270, 1996.

[34] M. R. Hill *et al.*, "A theoretical and non-destructive experimental approach for direct inclusion of measured collagen orientation and recruitment into mechanical models of the artery wall," *J. Biomech.*, vol. 45, pp. 762–771, 2012.

[35] M. S. Sacks, "Incorporation of experimentally-derived fiber orientation into a structural constitutive model for planar collagenous tissues," *J. Biomech. Eng.*, vol. 125, pp. 280–287, 2003.

[36] H. Chen *et al.*, "Biaxial deformation of collagen and elastin fibers in coronary adventitia," *J. Appl. Physiol.*, vol. 115, pp. 1683–1693, 2013.

[37] R. Rezakhaniha *et al.*, "Experimental investigation of collagen waviness and orientation in the arterial adventitia using confocal laser scanning microscopy," *Biomech. Model Mechanobiol.*, vol. 11, pp. 461–473, 2012.

[38] T. C. Gasser *et al.*, "Hyperelastic modelling of arterial layers with distributed collagen fibre orientations," *J. R. Soc. Interface.*, vol. 3, pp. 15–35, 2006.